Journal of Peptide Science
J. Pept. Sci. 2008; **14**: 1096–1102
Published online 18 June 2008 in Wiley InterScience (www.interscience.wiley.com). DOI: 10.1002/psc.1046

JOURNAL OF PEPTIDE SCIENCE

Structural characterization of a neurotoxic threonine-rich peptide corresponding to the human prion protein α2-helical 180–195 segment, and comparison with full-length α2-helix-derived peptides‡

LUISA RONGA,[a] PASQUALE PALLADINO,[a] GABRIELLA SAVIANO,[b] TEODORICO TANCREDI,[c] ETTORE BENEDETTI,[a] RAFFAELE RAGONE,[d] and FILOMENA ROSSI[a]*

[a] Dipartimento delle Scienze Biologiche and C.I.R.Pe.B., Università Federico II di Napoli, Naples, Italy
[b] Dipartimento di Scienze e Tecnologie per l'Ambiente e il Territorio, Università del Molise, Pesche, Italy
[c] Istituto di Chimica Biomolecolare, CNR, Pozzuoli, Italy
[d] Dipartimento di Biochimica e Biofisica and CRISCEB, Seconda Università di Napoli, Naples, Italy

Received 7 February 2008; *Revised 22 April 2008*; *Accepted 22 April 2008*

Abstract: The 173–195 segment corresponding to the helix 2 of the globular PrP domain is a good candidate to be one of the several 'spots' of intrinsic structural flexibility, which might induce local destabilization and concur to protein transformation, leading to aggregation-prone conformations. Here, we report CD and NMR studies on the α2-helix-derived peptide of maximal length (hPrP[180–195]) that is able to exhibit a regular structure different from the prevalently random arrangement of other α2-helix-derived peptides. This peptide, which has previously been shown to be affected by buffer composition via the ion charge density dependence typical of Hofmeister effects, corresponds to the *C*-terminal sequence of the PrP^{C} full-length α2-helix and includes the highly conserved threonine-rich 188–195 segment. At neutral pH, its conformation is dominated by β-type contributions, which only very strong environmental modifications are able to modify. On TFE addition, an increase of α-helical content can be observed, but a fully helical conformation is only obtained in neat TFE. However, linking of the 173–179 segment, as occurring in wild-type and mutant peptides corresponding to the full-length α2-helix, perturbs these intrinsic structural propensities in a manner that depends on whether the environment is water or TFE. Overall, these results confirm that the 180–195 parental region in $hPrP^{C}$ makes a strong contribution to the chameleon conformational behavior of the segment corresponding to the full-length α2-helix, and could play a role in determining structural rearrangements of the entire globular domain. Copyright © 2008 European Peptide Society and John Wiley & Sons, Ltd.

Keywords: prion protein; α2-helix; β-sheet; amyloid; transmissible spongiform encephalopathies; CD titration; NMR structure; prion toxicity

INTRODUCTION

Although its function is still largely unknown, the PrP is unequivocally associated with the onset of a family of diseases named transmissible spongiform encephalopathies (TSEs) [1] by a mechanism involving the isomerization of a soluble cellular form, PrP^{C}, whose structure basically consists of a leading unstructured tail linked to a *C*-terminus globular domain, containing three α-helices and a short two-stranded β-sheet [2–10], into an insoluble scrapie variant, PrP^{Sc}, deemed to retain intrinsic infectivity and characterized by a significant amount of β-structure [11]. Accordingly, it has been suggested that prion diseases proceed from a major misfolding event that leads to proteinase K-resistant amyloidogenic, β-sheet-containing and potentially infective structural variants [12–14], but hypotheses on the role played by such variants in prion aetiopathogenesis and on the link between amyloid-forming tendency and disease invariably have to face vagueness of information about the PrP^{Sc} structure [15–18].

Several studies have focused on the implication of the globular domain in the rearrangement mechanism and in the formation of toxic fibrils [19–25]. Particularly fascinating is the notion that the protein possesses one or several 'spots' of intrinsic conformational weakness, which may lead the whole secondary and tertiary structure to succumb in favor of more stable, but aggregation-prone conformations, depending on pH, redox condition, and glycosylation state [22,23]. The 173–195 segment corresponding to the helix 2 of the globular prion protein domain is a good candidate to be one of such spots. Indeed, the segments 176–183 and 185–193 have been predicted to possess strong amyloid- and β-structure-forming propensities,

Abbreviations: PrP, prion protein; PrP^{C}, cellular PrP; PrP^{Sc}, scrapie PrP; hPrP, human PrP; SDS, sodium dodecyl sulfate; TFE, 2,2,2-trifluoroethanol.

*Correspondence to: Filomena Rossi, Dipartimento delle Scienze Biologiche, Università 'Federico II' di Napoli, Via Mezzocannone 16, 80134 Napoli, Italy; e-mail: filomena.rossi@unina.it

‡Data deposition : AutoDep EBI-29054 with PDB ID code 2iv6 for coordinate entry.

Copyright © 2008 European Peptide Society and John Wiley & Sons, Ltd.

respectively [26], and the peptide encompassing the entire α2-helical segment has been shown to display conformational duality [27], a behavior that could be imputed to the frustrated helical state of the highly conserved threonine-rich *C*-terminal segment 188–195 [27–32]. Furthermore, the peptides 180–193 and 178–193 are the only ones that form an amyloid structure, according to data obtained by electron microscopy and Congo red birefringence [33], and other α2-helical fragments have been found to be toxic to neuronal cells and strongly fibrillogenic in a variety of conditions [19–21], adding a further clue to the working hypothesis that the α2-helix is involved in protein aggregation and scrapie-associated toxicity. As a matter of fact, several disease-causing point mutations are also gathered on this fragment, notably the D178N, V180I, T183A, H187R, T188R, T188K, and T188A, which are presumed to induce local destabilization, thus contributing to protein transformation [34–36].

On this ground, we have devoted several efforts to the study of peptides derived from the human full-length helix 2, and stressed on several occasions that their functional and structural properties are compatible with the involvement of the parental sequence in the conversion of PrP^{C} to PrP^{Sc} [9,10,27,32,37]. Interestingly, recent studies suggest that the conformational conversion of PrP^{C} involves major refolding of the *C*-terminal α-helical region [38] and map the β-sheet core of PrP amyloid to the *C*-terminal region that in the native structure of monomeric PrP^{C} corresponds to α-helix 2, a major part of α-helix 3, and the loop between these two helices [39].

We have previously found that, in aqueous solution, the CD spectra of the PrP^{C} wild-type peptide and the Creutzfeldt-Jakob-disease-associated mutant, both derived from the full-length α-helix 2 (hPrP[173–195] and hPrP[173–195]D178N, respectively) are dominated by disordered structure [9,10]. Eventually, we have characterized the α-helical organization of these peptides in an α-helix-inducing environment [37]. In the present study, we broaden our horizons to a model peptide that does not include the 173–179 segment, hPrP[180–195], thus corresponding to the 180–195 *C*-terminal sequence of the PrP α2-helix. This peptide is devoid of effects linked to the reactivity of the thiolic cysteine side chain, includes the highly conserved threonine-rich 188–195 *C*-terminal part of the PrP^{C} full-length helix 2, to which the conformational ambivalence of the helix 2 has been attributed, and has already been shown to be affected by buffer composition via the ion charge density dependence typical of Hofmeister effects [40]. Here, we further investigate its conformational behavior in solution.

MATERIALS AND METHODS

Chemicals

HPLC chemicals were purchased from Lab-Scan (Dublin, Ireland), and the remainder of organic reagents were from Sigma-Aldrich (Milan, Italy). All solvents were reagent grade. N^{α}-Fmoc-protected amino acids and activating agents were purchased from Inbios (Pozzuoli, Italy). Resin for peptide synthesis was from Novabiochem (Läufelfingen, Switzerland). Columns for peptide purification and characterization were from Phenomenex (Torrance, CA, USA). SDS and TFE were obtained from Sigma-Aldrich (Milano, Italia) and Romil LTD (Dublin, Ireland), respectively.

Peptide Synthesis

The N- and C-blocked Ac-NNFVHDC-NH_2 and Ac-VNITIKQHTV TTTTKG-NH_2 peptides, henceforth identified as hPrP[173–179] and hPrP[180–195], corresponding to the 173–179 and 180–195 segments in the PrP full-length helix 2, respectively, were synthesized in batch by standard 9-fluorenylmethyl carbamate chemistry protocol using Rink-amide MBHA resin. After peptide assembling, acetylation was carried out by 1 M acetic anhydride in dimethylformamide containing 5% *N*,*N*-diisopropyl ethylamine. Fmoc-synthesized peptides were then cleaved from the solid support by treatment with trifluoroacetic acid/triisopropylsilane/water (TFA/TIS/H_2O, 9 : 0.5 : 0.5 v/v/v) mixture for 90 min at room temperature, precipitated in ether, dissolved in water/acetonitrile (1 : 1 v/v) mixture, lyophilized and purified by RP-HPLC using a C_{18} Jupiter (250 × 22 mm) column with a linear gradient of acetonitrile (10–60%) in 0.1% TFA at room temperature. Peptide purity and integrity were confirmed by LC-MS technique (Finnigan Surveyor, Thermo Electron Corporation).

Circular Dichroism

Far UV CD spectra were recorded from 190 to 260 nm on a Jasco J-715 spectropolarimeter at 20 °C, using 1-cm quartz cell containing 20 μM peptide dissolved in 10 mM phosphate buffer. Each spectrum was obtained averaging three scans, subtracting contributions from other species in solution, and converting the signal to mean residue ellipticity in units of deg cm^2 $dmol^{-1}$ res^{-1}. Other experimental settings were 20 nm/min-scan speed, 2.0-nm band width, 0.2-nm resolution, 50-mdeg sensitivity, and 4-s response. Preliminary experiments were also carried out to exclude the occurrence of self-association effects. To this aim, equimolecular spectra of hPrP[180–195] solutions were acquired for each subsequent dilution of a series obtained from a 10^{-4} M stock solution. The dilution factor was then used to calculate the cell pathlength that was necessary to keep constant the number of peptide molecules in the optical path. Under these conditions, signal constancy is expected in the absence of self-association, which may cause hyperbolic deviations from the Beer–Lambert's law because of concomitant secondary structure rearrangements. SDS and TFE titrations were carried out under the same experimental conditions as above. In particular, SDS experiments were based on the notion that peptides may be induced into a β-structure at submicellar SDS concentrations [41–43]. Small surfactant

Copyright © 2008 European Peptide Society and John Wiley & Sons, Ltd.

DOI: 10.1002/psc

aliquots were therefore added from a stock solution up to a final concentration equal to the critical micellar concentration (cmc) at room temperature (4 mM) [44–46].

NMR Experiments and Structure Calculations

NMR experiments were performed by dissolving 2 mM peptide in TFEd2-OH (99%). NMR spectra were acquired at 300 K on a 600-MHz Bruker Avance spectrometer equipped with a cryoprobe. The peptide TOCSY spectra showed well-resolved resonances for almost all residues, and sequence specific assignment was obtained by the combined use of TOCSY and NOESY experiments, according to the standard procedure [37,47].

NOESY spectra at 300-ms mixing time were used for the integration of NOE cross peaks. Peak integrals were evaluated by NMRView, transferred to the program package DYANA 1.0.6 [48], and converted to upper distance limits by using the CALIBA [49] module of DYANA. Distance constraints were then worked out by the GRIDSEARCH module to generate a set of allowed dihedral angles. Structure calculation was carried out with the macro ANNEAL module by torsion angle dynamics. Eighty structures were calculated by TSSA, starting with a total of 10 000 MD steps and a default value of maximum temperature. The 30 best structures in terms of target functions were considered. A total of 118 distance restraints were used for the structure calculation of hPrP[180–195]. These restraints, derived from interresidue, sequential and medium range NOEs, were introduced in the SA torsion space calculation performed by the DYANA package. The best 30 structures in terms of root mean square deviation (RMSD) were selected from 80 structures sampled in TSSA calculations.

Biological Assays

The neurotoxicity of α2-helix-derived peptides was assayed on B104 neuroblastoma cells from rat central nervous system [50], cultured in Dulbecco's modified Eagle's minimal essential medium and exposed to 0–240 μM peptide concentrations. Cell survival was assessed by comparison with untreated control cultures after a 48-h exposure, and expressed as 50% fatal concentration (FC_{50}).

RESULTS AND DISCUSSION

In the preliminary experiments, we have performed equimolecular CD spectra of hPrP[180–195] to exclude effects caused by self-association and/or aggregation phenomena. As depicted in Figure 1, the observed ellipticity is constant below 50 μM, which indicates that hPrP[180–195] is monomeric in the 0–50 μM range, whereas the intensity decrease occurring above 50 μM is associated with peptide aggregation.

Owing to the above-described aggregation effects, information on the conformational behavior in aqueous solution mostly comes from CD spectra. As the CD spectra of hPrP[180–195] and hPrP[173–179] (Figure 2) are dominated by β-type contributions and random organization, respectively, it seems reasonable to infer that, in previously characterized wild-type and

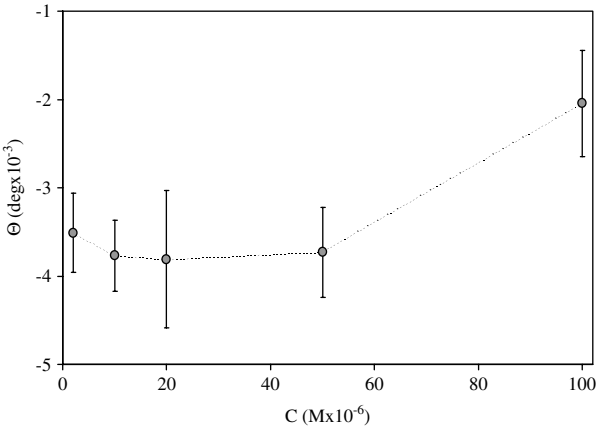

Figure 1 Ellipticity of hPrP[180–195] solutions. Equimolecular spectra were acquired for each subsequent dilution of a series obtained from a concentrated mother solution in phosphate buffer, pH 7. For each solution, the dilution factor was used to calculate the cell pathlength to be used to keep constant the number of peptide molecules in the optical path. Under these conditions, signal constancy at 200 nm monitors the absence of self-association.

mutant peptides corresponding to the entire α2-helical segment (hPrP[173–195] and hPrP[173–195]D178N, respectively, [37]), the scarcity of the ordered structure is associated with the presence of the 173–179 segment. As a matter of fact, CD spectra of hPrP[173–195] and hPrP[173–195]D178N, both of which include the 173–179 segment, do not show the β-type peculiarities exhibited by hPrP[180–195] [9,10]. It can be also appreciated from Table 1 that the structural organization of peptides is not related to their neuronal toxicity, but the presence of the 180–195 sequence is associated to much lower FC_{50}s. On this basis, hPrP[180–195] appears to be the α-helix 2-derived peptide of maximal length with intrinsic propensity to be organized in a regular structure. Although the 180–195 segment is not able to retain the regular organization shown by hPrP[180–195] when it is embedded in peptides dominated by random organization, its intrinsic structural propensity appears to play a role in determining their biological properties.

The addition of submicellar SDS caused a marked increase of the positive band near 200 nm in the spectrum of hPrP[180–195] (Figure 3(A)), suggesting enhancement of the β-type features that were already present in the peptide. There is a large body of literature about the nature of this solvent system, which has been described as a mimetic of protein interiors. It is commonly accepted that the nonpolar tails provide a template for the hydrophobic domains of peptides, mimicking the environment experienced in the protein interior, whereas the sulfate moiety is able to keep the β-structured peptide in solution. Peptide–SDS association data were then treated with the five-parameter equation:

Copyright © 2008 European Peptide Society and John Wiley & Sons, Ltd.

DOI: 10.1002/psc

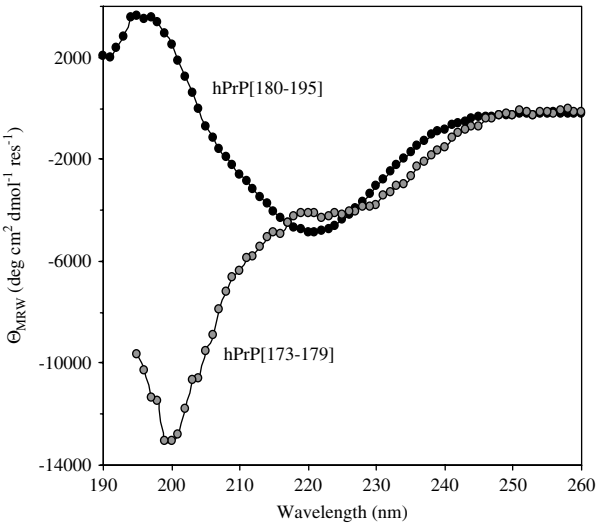

Figure 2 Far UV CD spectra. The concentration of hPrP[180–195] (black symbols) and hPrP[173–179] (gray symbols) was 20 μM in 10 mM phosphate buffer at neutral pH.

$$\Theta_{200} = \{\Theta_o + \Theta_f \exp[-\Delta G^\circ/(RT) + \Delta n \ln(1 + kD)]\}/ \{1 + \exp[-\Delta G^\circ/(RT) + \Delta n \ln(1 + kD)]\} \quad (1)$$

This model was originally derived to evaluate free energy changes for the disorder-to-order transition of hPrP[173–195] by extrapolating isothermal titration data to zero concentration of SDS [27]. Here, the surfactant concentration is given by D, and Θ_o and Θ_f represent the initial and final dichroic signal values, respectively. The free energy of secondary structure formation in the absence of SDS is given by ΔG°, and Δn represents the excess of the surfactant binding sites in the saturated state characterized by the intrinsic binding constant k. Curve fitting was carried out fixing $k = 50\,000\ \text{M}^{-1}$, which is the value found for SDS interaction with electrostatic binding sites of small proteins [51], and Θ_o and Θ_f at their respective experimental values. The ΔG° and Δn values resulting from this fitting procedure (correlation = 0.994) were 24.3 ± 7.5 kJ/mol and 2.5 ± 0.7 sites, respectively (estimated value ± standard deviation). Notably, the value of Δn well agrees with the number of potentially charged residues present in hPrP[180–195] (namely, two lysines and one histidine). NMR evidence of whether or not SDS is acting like a protein core could not be obtained because of extensive aggregation on raising the peptide concentration.

Very strong environmental modifications were necessary to modify the marked preference of hPrP[180–195] for a β-type conformation. Indeed, both pH decrease and temperature increase caused conversion into prevalently random organization, and the thermal transition was even accompanied by extensive aggregation (data not shown). The conformational arrangement that hPrP[180–195] is able to assume at neutral pH, even in the absence of SDS, suggests that the 180–195 parental region in $hPrP^C$ makes a strong contribution to the chameleon conformational behavior of the segment corresponding to the full-length α2-helix [27], and could play a role in determining the structural rearrangements of the entire globular domain. However, on TFE addition (≤50%), an increase of α-helical content could be observed, as testified by the appearance of a shoulder around 208 nm (Figure 3(B)), but a fully helical conformation was obtained only in neat TFE.

TFE is well known for its α-helix-inducing properties. We have already reported [37] that, using TFE as a mimetic of the PrP^C interior, hPrP[173–195] adopts the helical conformation that is fully observed in the native protein, whereas the conformation of the hPrP[173–195]D178N mutant is modified into a bent structure formed by two helices separated by a kink centered on Lys185 and Gln186. This suggests that structural weaknesses occurring in the N-terminal 173–179 region, such as the D178N substitution that we have examined, may lead to partial unwinding of the helical conformation of the 180–195 segment in a native-like environment. Hence, also considering that, in aqueous solution, the 173–179 region has been shown to disfavor the occurrence of a regular structure in the remaining part of the entire α2-helix-derived

Table 1 Secondary structure and neurotoxicity of α2-helix-derived peptides

Peptide	Secondary structure (phosphate buffer, pH 7)	FC_{50} (μM)
hPrP[173–179] Ac-NNFVHDC-NH_2	Random	430
hPrP[180–195] Ac-VNITIKQHTVTTTTKG-NH_2	Beta	11
hPrP[173–195] Ac-NNFVHDCVNITIKQHTVTTTTKG-NH_2	Random	68
hPrP[173–195]D178N Ac-NNFVHNCVNITIKQHTVTTTTKG-NH_2	Random	12

Copyright © 2008 European Peptide Society and John Wiley & Sons, Ltd.

DOI: 10.1002/psc

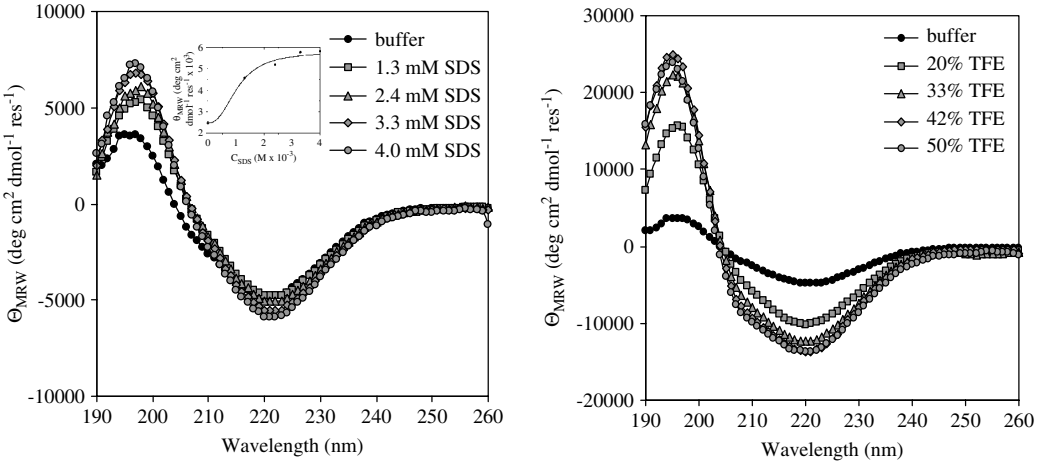

Figure 3 Effect of structuring agents on hPrP[180–195]. Increasing amounts of SDS and TFE were added to 20 μM peptide dissolved in 10 mM phosphate buffer, pH 7. Final spectra were corrected for dilution. The inset shows best fitting of SDS binding data to Eqn (1) (ellipticity at 200 nm, see text for details). The fitting procedure was performed implementing this equation in the general-purpose nonlinear fitting program Scientist from MicroMath Software (San Diego, CA).

segment, as modeled by the hPrP[180–195] peptide, we have then used TFE to investigate whether this region may play a role in affecting the intrinsic conformational propensity of the isolated 180–195 segment even under a nativelike condition.

Indeed, as shown in Figure 4, strong $d_{NN(i,i+1)}$ sequential and $d_{\alpha\beta(i,i+3)}$ medium range effects derived from the NOESY spectrum of hPrP[180–195] dissolved in TFE were typical of α-helical structure, and a similar suggestion comes from the bundle of the region 182–191 of the best 30 DYANA structures sampled in TSSA calculations. This provides direct evidence that the 180–195 segment possesses an intrinsic ability to adopt a fully helical conformation in TFE, but, when compared with the data summarized above, indirectly suggests that the modification of the 173–179 region, as occurring in hPrP[173–195]D178N, plays a role in determining the unwinding of its helical arrangement. In other words, the intrinsic propensity of the 180–195 region to adopt regular conformation appears to be strongly affected by the presence of the 173–179 region, which is able to perturb the organization of the whole α2-helical segment in a manner that depends on whether the environment is water (nonnative) or TFE (nativelike).

Figure 4 NOE effects and DYANA backbone fitting of hPrP[180–195]. Connectivities were derived from NOESY spectra at 300-ms mixing time. Backbone NOE connectivities are indicated by horizontal lines between residues, with thickness indicating their relative magnitude. The first three lines below the amino acid sequence represent torsion angle restraints for the backbone torsion angles ϕ and ψ, and for the side-chain torsion angle χ_1. For ϕ and ψ, | symbols enclose secondary-structure-type conformation; ▲ symbols indicate compatibility with an ideal α-helix; ▼ are used for torsion angles compatible with β-strand; and a ● symbol marks a restraint that excludes the torsion angle values of these regular secondary structure elements. Filled squares of different sizes depict torsion angle restraints for χ_1, depending on the number of allowed staggered rotamer positions. The bundle of the region 182–191 of the best 30 DYANA structures was obtained by best fitting of the backbone (RMSD = 0.45 ± 0.25 Å).

CONCLUSIONS

It is currently believed that the major structural modifications involved in the PrP protein misfolding are located in the structureless *N*-terminal region, and a number of models have been proposed [52–55]. However, several investigations methodically neglect a possible involvement of the globular domain, and sometimes are not devoid of contradiction, so that any definite conclusion cannot be made yet [53–57].

On the other hand, we have reported on several occasions that functional and structural properties of peptides derived from the human full-length helix 2 are compatible with the involvement of this segment in the conversion of PrP^C to PrP^{Sc} [9,10,27,32,37], and recent studies have finally turned their attention to the *C*-terminal α-helical region [38,39]. Although the organization of helix 1 and helix 3 is preserved in

Copyright © 2008 European Peptide Society and John Wiley & Sons, Ltd.

DOI: 10.1002/psc

the whole PrP architecture, likely because of their intrinsic structural stability [31,56,58,59], the other side of the coin is that conformational ambiguity makes the structural arrangement of the segment corresponding to helix 2 strongly dependent on the environment [21,27,60–63]. Here, we have shown that the *C*-terminal α2-helical 180–195 region possesses intrinsic propensity to adopt β- and α-conformation in water and TFE, respectively, but its organization is dominated by the *N*-terminal 173–179 segment, although through different mechanisms, both in water and in TFE. This adds a further clue to the hypothesis that the segment corresponding to helix 2 is implicated in the mechanism of anomalous PrP folding, as can be also inferred from an analysis of the PrP pathological variants [64–67] and from its recently reported ease of unwinding [68].

Acknowledgements

This work has been supported by funds from the Ministero dell'Università e della Ricerca (M.U.R.). The authors acknowledge Dr Giuseppe Perretta (IBB-CNR, Naples) for technical assistance and Prof. Michele Maffia and Dr Emanuela Urso (University of Lecce, Italy) for biological tests.

REFERENCES

1. Cohen FE, Prusiner SB. Pathologic conformations of prion proteins. *Annu. Rev. Biochem.* 1998; **67**: 793–819.
2. Riek R, Hornemann S, Wider G, Billeter M, Glockshuber R, Wüthrich K. NMR structure of the mouse prion protein domain PrP(121–321). *Nature* 1996; **382**: 180–182.
3. Zahn R, Liu A, Lührs T, Riek R, von Schroetter C, Garcia FL, Billeter M, Calzolai L, Wider G, Wüthrich K. NMR solution structure of the human prion protein. *Proc. Natl. Acad. Sci. U.S.A.* 2000; **97**: 145–150.
4. López Garcia F, Zahn R, Riek R, Wüthrich K. NMR structure of the bovine prion protein. *Proc. Natl. Acad. Sci. U.S.A.* 2000; **97**: 8334–8339.
5. Pérez DR, Wüthrich K. NMR assignment of the Xenopus laevis prion protein fragment xlPrP (98-226). *J. Biomol. NMR* 2005; **31**: 260–260.
6. Lysek DA, Schorn C, Nivon LG, Esteve-Moya V, Christen B, Calzolai L, von Schroetter C, Fiorito F, Herrmann T, Güntert P, Wüthrich K. Prion protein NMR structures of cats, dogs, pigs, and sheep. *Proc. Natl. Acad. Sci. U.S.A.* 2005; **102**: 640–645.
7. Gossert AD, Bonjour S, Lysek DA, Fiorito F, Wüthrich K. Prion protein NMR structures of elk and of mouse/elk hybrids. *Proc. Natl. Acad. Sci. U.S.A.* 2005; **102**: 646–650.
8. Calzolai L, Lysek DA, Pérez DR, Güntert P, Wüthrich K. Prion protein NMR structures of chickens, turtles, and frogs. *Proc. Natl. Acad. Sci. U.S.A.* 2005; **102**: 651–655.
9. Ronga L, Tizzano B, Palladino P, Ragone R, Urso E, Maffia M, Ruvo M, Benedetti E, Rossi F. The prion protein: structural features and related toxic peptides. *Chem. Biol. Drug Des.* 2006; **68**: 139–147.
10. Ronga L, Palladino P, Costantini S, Facchiano A, Ruvo M, Benedetti E, Ragone R, Rossi F. Conformational diseases and structure-toxicity relationships: lessons from prion-derived peptides. *Curr. Protein Pept. Sci.* 2007; **8**: 83–90.
11. Legname G, Baskalov IV, Nguyen H-OB, Riesner D, Cohen FE, DeArmond SJ, Prusiner SB. Synthetic mammalian prions. *Science* 2004; **305**: 673–676.
12. Prusiner SB. Prions. *Proc. Natl. Acad. Sci. U.S.A.* 1998; **95**: 13363–13383.
13. Kelly JW. The alternative conformations of amyloidogenic proteins and their multi-step assembly pathways. *Curr. Opin. Struct. Biol.* 1998; **8**: 101–106.
14. Scott MR, Will R, Ironside J, Nguyen H-OB, Tremblay P, DeArmond SJ, Prusiner SB. Compelling transgenetic evidence for transmission of bovine spongiform encephalopathy prions to humans. *Proc. Natl. Acad. Sci. U.S.A.* 1999; **96**: 15137–15142.
15. Kaneko K, Zulianello L, Scott M, Cooper CM, Wallace AC, James TL, Cohen FE, Prusiner SB. Evidence for protein X binding to a discontinuous epitope on the cellular prion protein during scrapie prion propagation. *Proc. Natl. Acad. Sci. U.S.A.* 1997; **94**: 10069–10074.
16. Perrier V, Wallace AC, Kaneko K, Safar J, Prusiner SB, Cohen FE. Mimicking dominant negative inhibition of prion replication through structure-based drug design. *Proc. Natl. Acad. Sci. U.S.A.* 2000; **97**: 6073–6078.
17. Kazlauskaite J, Sanghera N, Sylvester I, Vénien-Brian C, Pinheiro TJT. Structural changes of the prion protein in lipid membranes leading to aggregation and fibrillization. *Biochemistry* 2003; **42**: 3295–3304.
18. Critchley P, Kazlauskaite J, Eason R, Pinheiro TJT. Binding of prion proteins to lipid membranes. *Biochem. Biophys. Res. Commun.* 2004; **313**: 559–567.
19. Gasset M, Baldwin MA, Lloyd DH, Gabriel J-M, Holtzman DM, Cohen F, Fletterick R, Prusiner SB. Predicted α-helical regions of the prion protein when synthesized as peptides form amyloid. *Proc. Natl. Acad. Sci. U.S.A.* 1992; **89**: 10940–10944.
20. Jackson GS, Hosszu LL, Power A, Hill AF, Kenney J, Saibil H, Craven CJ, Waltho JP, Clarke AR, Collinge J. Reversible conversion of monomeric human prion protein between native and fibrillogenic conformations. *Science* 1999; **283**: 1935–1937.
21. Horiuchi M, Baron GS, Xiong LW, Caughey B. Inhibition of interactions and interconversions of prion protein isoforms by peptide fragments from the C-terminal folded domain. *J. Biol. Chem.* 2001; **276**: 15489–15497.
22. Ma J, Wollmann R, Lindquist S. Neurotoxicity and neurodegeneration when PrP accumulates in the cytosol. *Science* 2002; **298**: 1781–1785.
23. Bosques CJ, Imperiali B. The interplay of glycosylation and disulfide formation influences fibrillization in a prion protein fragment. *Proc. Natl. Acad. Sci. U.S.A.* 2003; **100**: 7593–7598.
24. Brown DR, Guantieri V, Grasso G, Impellizzeri G, Pappalardo G, Rizzarelli E. Copper(II) complexes of peptide fragments of the prion protein. Conformation changes induced by copper(II) and the binding motif in C-terminal protein region. *J. Inorg. Biochem.* 2004; **98**: 133–143.
25. DuBay KF, Pawar AP, Chiti F, Zurdo J, Dobson CM, Vendruscolo M. Prediction of the absolute aggregation rates of amyloidogenic polypeptide chains. *J. Mol. Biol.* 2004; **341**: 1317–1326.
26. Galzitskaya OV, Garbuzynskiy SO, Lobanov MY. Prediction of amyloidogenic and disordered regions in protein chains. *PLoS Comput. Biol.* 2006; **2**: 1639–1648.
27. Tizzano B, Palladino P, De Capua A, Marasco D, Rossi F, Benedetti E, Pedone C, Ragone R, Ruvo M. The human prion protein α2 helix: a thermodynamic study of its conformational preferences. *Proteins* 2005; **59**: 72–79.
28. Dima RI, Thirumalai D. Exploring the propensities of helices in PrP^C to form β sheet using NMR structures and sequence alignments. *Biophys. J.* 2002; **83**: 1268–1280.
29. Dima RI, Thirumalai D. Probing the instabilities in the dynamics of helical fragments from mouse PrP^C. *Proc. Natl. Acad. Sci. U.S.A.* 2004; **101**: 15335–15340.
30. Langella E, Improta R, Barone V. Checking the pH-induced conformational transition of prion protein by molecular dynamics

Copyright © 2008 European Peptide Society and John Wiley & Sons, Ltd.

simulations: effect of protonation of histidine residues. *Biophys. J.* 2004; **87**: 3623–3632.
31. Colacino S, Tiana G, Broglia RA, Colombo G. The determinants of stability in the human prion protein: insights into folding and misfolding from the analysis of the change in the stabilization energy distribution in different conditions. *Proteins* 2006; **62**: 698–707.
32. Ronga L, Langella E, Palladino P, Marasco D, Tizzano B, Saviano M, Pedone C, Improta R, Ruvo M. Does tetracycline bind helix 2 of prion? An integrated spectroscopical and computational study of the interaction between the antibiotic and α helix 2 human prion protein fragments. *Proteins* 2007; **66**: 707–715.
33. Thompson A, White AR, McLean C, Masters CL, Cappai R, Barrow CJ. Amyloidogenicity and neurotoxicity of peptides corresponding to the helical regions of PrP(C). *J. Neurosci. Res.* 2000; **62**: 293–301.
34. Prusiner SB. Molecular biology and pathogenesis of prion diseases. *Trends Biochem. Sci.* 1996; **21**: 482–487.
35. Shamsir MS, Dalby AR. One gene, two diseases and three conformations: molecular dynamics simulations of mutants human prion protein at room temperature and elevated temperatures. *Proteins* 2005; **59**: 275–290.
36. Gsponer J, Ferrara P, Caflisch A. Flexibility of the murine prion protein and its Asp178Asn mutant investigated by molecular dynamics simulations. *J. Mol. Graph. Model.* 2001; **20**: 169–182.
37. Ronga L, Palladino P, Saviano G, Tancredi T, Benedetti E, Ragone R, Rossi F. NMR structure and CD titration with metal cations of human prion α2-helix-related peptides. *Bioinorg. Chem. Appl.* 2007; 10720. DOI: 10.1155/2007/10720.
38. Cobb NJ, Sönnichsen FD, McHaourab H, Surewicz WK. Molecular architecture of human prion protein amyloid: a parallel, in-register beta-structure. *Proc. Natl. Acad. Sci. U.S.A.* 2007; **104**: 18946–18951.
39. Lu X, Wintrode PL, Surewicz WK. β-sheet core of human prion protein amyloid fibrils as determined by hydrogen/deuterium exchange. *Proc. Natl. Acad. Sci. U.S.A.* 2007; **104**: 1510–1515.
40. Ronga L, Palladino P, Tizzano B, Marasco D, Benedetti E, Ragone R, Rossi F. Effect of salts on the structural behavior of hPrP alpha2-helix-derived analogues: the counterion perspective. *J. Pept. Sci.* 2006; **12**: 790–795.
41. Wu CS, Ikeda K, Yang JT. Ordered conformation of polypeptides and proteins in acidic dodecyl sulfate solution. *Biochemistry* 1981; **20**: 566–570.
42. Wu CS, Yang JT. Sequence-dependent conformations of short polypeptides in a hydrophobic environment. *Mol. Cell. Biochem.* 1981; **40**: 109–122.
43. Zhong L, Johnson WC Jr. Environment affects amino acid preference for secondary structure. *Proc. Natl. Acad. Sci. U.S.A.* 1992; **89**: 4462–4465.
44. Esposito C, Colicchio P, Facchiano A, Ragone R. Effect of a weak electrolyte on the critical micellar concentration of sodium dodecyl sulfate. *J. Colloid Interface Sci.* 1998; **200**: 310–312.
45. Le Maire M, Champeil P, Møller JV. Interaction of membrane proteins and lipids with solubilizing detergents. *Biochim. Biophys. Acta* 2000; **1508**: 86–111.
46. Kuroda Y, Maeda Y, Sawa S, Shibata K, Miyamoto K, Nakagawa T. Effects of detergents on the secondary structures of prion protein peptides as studied by CD spectroscopy. *J. Pept. Sci.* 2003; **9**: 212–220.
47. Wüthrich K. *NMR of Proteins and Nucleic Acids*. Wiley: New York, 1986.
48. Güntert P, Braun W, Wüthrich K. Efficient computation of three-dimensional protein structures in solution from nuclear magnetic resonance data using the program DIANA and the supporting programs CALIBA, HABAS and GLOMSA. *J. Mol. Biol.* 1991; **217**: 517–530.
49. Güntert P, Mumenthaler C, Wüthrich K. Torsion angle dynamics for NMR structure calculation with the new program DYANA. *J. Mol. Biol.* 1997; **273**: 283–298.
50. Schubert D, Heinemann S, Carlisle W, Tarikas H, Kimes B, Patrick J, Steinbach JH, Culp W, Brandt BL. Clonal cell lines from the rat central nervous system. *Nature* 1974; **249**: 224–227.
51. Bordbar AK, Saboury AA, Housaindokht MR, Moosavi-Movahedi AA. Statistical effects of the binding of ionic surfactant to protein. *J. Colloid Interface Sci.* 1997; **192**: 415–419.
52. Wille H, Michelitsch MD, Guénebaut V, Supattapone S, Serban A, Cohen FE, Agard DA, Prusiner SB. Structural studies of the scrapie prion protein by electron crystallography. *Proc. Natl. Acad. Sci. U.S.A.* 2002; **99**: 3563–3568.
53. Govaerts C, Wille H, Prusiner SB, Cohen FE. Evidence for assembly of prions with left-handed α-helices into trimers. *Proc. Natl. Acad. Sci. U.S.A.* 2004; **101**: 8342–8347.
54. Yang S, Levine H, Onuchic JN, Cox DL. Structure of infectious prions: stabilization by domain swapping. *FASEB J.* 2005; **19**: 1778–1783.
55. Eghiaian F, Grosclaude J, Lesceu S, Debey P, Doublet B, Tréguer E, Rezaei H, Knossow M. Insight into the $PrP^{C} \rightarrow PrP^{Sc}$ conversion from the structures of antibody-bound ovine prion scrapie-susceptibility variants. *Proc. Natl. Acad. Sci. U.S.A.* 2004; **101**: 10254–10259.
56. Ziegler J, Sticht H, Marx UC, Müller W, Rösch P, Schwarzinger S. CD and NMR studies of prion protein (PrP) helix 1. *J. Biol. Chem.* 2003; **278**: 50175–50181.
57. Cox DL, Pan J, Singh RRP. A mechanism for copper inhibition of infectious prion conversion. *Biophys. J.* 2006; **91**: L11–L13.
58. Gallo M, Paludi D, Cicero DO, Chiovitti K, Millo E, Salis A, Damonte G, Corsaro A, Thellung S, Schettini G, Melino S, Florio T, Paci M, Aceto A. Identification of a conserved N-capping box important for the structural autonomy of the prion α3-helix: the disease associated D202N mutation destabilizes the helical conformation. *Int. J. Immunol. Pharmacol.* 2005; **18**: 95–112.
59. Watzlawik J, Skora L, Frense D, Griesinger C, Zweckstetter M, Schultz-Schaeffer WJ, Kramer ML. Prion protein helix1 promotes aggregation but is not converted into β-sheet. *J. Biol. Chem.* 2006; **281**: 30242–30250.
60. Calzolai L, Zahn R. Influence of pH on NMR structure and stability of the human prion protein globular domain. *J. Biol. Chem.* 2003; **278**: 35592–35596.
61. Haire LF, Whyte SM, Vasisht N, Gill AC, Verma C, Dodson EJ, Dodson GG, Bayley PM. The crystal structure of the globular domain of sheep prion protein. *J. Mol. Biol.* 2004; **336**: 1175–1183.
62. Knaus KJ, Morillas M, Swietnicki W, Malone M, Surewicz WK, Yee VC. Crystal structure of the human prion protein reveals a mechanism for oligomerization. *Nat. Struct. Biol.* 2001; **8**: 770–774.
63. Lee S, Eisenberg D. Seeded conversion of recombinant prion protein to a disulfide-bonded oligomer by a reduction-oxidation process. *Nat. Struct. Biol.* 2003; **10**: 725–730.
64. Jackson GS, Collinge J. The molecular pathology of CJD: old and new variants. *Mol. Pathol.* 2001; **54**: 393–399.
65. Gasteiger E, Gattiker A, Hoogland C, Ivanyi I, Appel RD, Bairoch A. ExPASy: the proteomics server for in-depth protein knowledge and analysis. *Nucleic Acids Res.* 2003; **31**: 3784–3788.
66. Kiachopoulos S, Bracher A, Winklhofer KF, Tatzelt J. Pathogenic mutations located in the hydrophobic core of the prion protein interfere with folding and attachment of the glycosylphosphatidylinositol anchor. *J. Biol. Chem.* 2005; **280**: 9320–9329.
67. Hirschberger T, Stork M, Schropp B, Winklhofer KF, Tatzelt J, Tavan P. Structural instability of the prion protein upon M205S/R mutations revealed by molecular dynamics simulations. *Biophys. J.* 2006; **90**: 3908–3918.
68. Fitzmaurice TJ, Burke DF, Hopkins L, Yang S, Yu S, Sy M-S, Thackray AM, Bujdoso R. The stability and aggregation of ovine prion protein associated with classical and atypical scrapie correlates with the ease of unwinding of helix-2. *Biochem. J.* 2008; **409**: 367–375.

Copyright © 2008 European Peptide Society and John Wiley & Sons, Ltd.